

Combining MRI with PET for partial volume correction improves image-derived input functions in mice

Eleanor Evans, Guido Buonincontri, David Izquierdo, Carmen Methner, Rob C. Hawkes, *Member, IEEE*, Richard E. Ansorge, Thomas Krieg, T. Adrian Carpenter, and Stephen J. Sawiak, *Member, IEEE*

Abstract— Accurate kinetic modelling using dynamic PET requires knowledge of the tracer concentration in plasma, known as the arterial input function (AIF). AIFs are usually determined by invasive blood sampling, but this is prohibitive in murine studies due to low total blood volumes. As a result of the low spatial resolution of PET, image-derived input functions (IDIFs) must be extracted from left ventricular blood pool (LVBP) ROIs of the mouse heart. This is challenging because of partial volume and spillover effects between the LVBP and myocardium, contaminating IDIFs with tissue signal. We have applied the geometric transfer matrix (GTM) method of partial volume correction (PVC) to 12 mice injected with ^{18}F -FDG affected by a Myocardial Infarction (MI), of which 6 were treated with a drug which reduced infarction size [1]. We utilised high resolution MRI to assist in segmenting mouse hearts into 5 classes: LVBP, infarcted myocardium, healthy myocardium, lungs/body and background. The signal contribution from these 5 classes was convolved with the point spread function (PSF) of the Cambridge split magnet PET scanner and a non-linear fit was performed on the 5 measured signal components. The corrected IDIF was taken as the fitted LVBP component. It was found that the GTM PVC method could recover an IDIF with less contamination from spillover than an IDIF extracted from PET data alone. More realistic values of K_i were achieved using GTM IDIFs, which were shown to be significantly different ($p < 0.05$) between the treated and untreated groups.

Index Terms— Arterial input function, Geometric transfer matrix, MRI, partial volume correction, small animal PET

E. Evans was funded by an MRC studentship and travel to PSMR 2014 was funded by the EU COST action for PET/MR.

E. Evans, R. Hawkes and T. A. Carpenter are with the Wolfson Brain Imaging Centre, University of Cambridge, Cambridge, UK, CB2 0QQ (e-mail: ee244@cam.ac.uk, rch20@cam.ac.uk and tac12@cam.ac.uk).

G. Buonincontri is with both the Wolfson Brain Imaging Centre and the Department of Medicine, University of Cambridge, Cambridge, UK, CB2 0QQ (e-mail: gb396@cam.ac.uk).

D. Izquierdo is with the Athinoula A. Martinos Center for Biomedical Imaging, 149 Thirteenth Street, Suite 2301, Charlestown, MA, 02129 (e-mail: davidizq@nmr.mgh.harvard.edu).

C. Methner was with the Department of Medicine, University of Cambridge and is now at Oregon Health and Science University, Portland, OR, 97239 (e-mail: cm618@medschl.cam.ac.uk).

R. E. Ansorge is with the Department of Physics, University of Cambridge, Cambridge, UK, CB3 0HE (e-mail: real@cam.ac.uk).

T. Krieg is a member of the Department of Medicine, University of Cambridge, Cambridge, UK, CB2 0QQ (e-mail: tk382@medschl.cam.ac.uk).

S. J. Sawiak is a member of both the Wolfson Brain Imaging Centre, and the Behavioural and Clinical Neurosciences Institute, University of Cambridge, Cambridge, UK, CB2 3EB (e-mail: sjs80@cam.ac.uk).

I. INTRODUCTION

POSITRON emission tomography (PET) is a quantitative imaging technique with very high sensitivity and specificity, making it ideally suited to functional imaging investigations. Image quantitation can be performed using standard uptake values (SUVs) [2] although the accuracy of such measures has been questioned [3] and the emphasis in small animal imaging has shifted towards the use of biomarkers obtained with compartmental modelling of tracer kinetics [4]. In murine studies, Fluorodeoxyglucose (^{18}F -FDG) is commonly used to quantify glucose metabolism in the brain [5] and heart [6], [7] by analysing the rate constants extracted from a two compartment model. Different models must be applied to suit the pharmacokinetics of each PET tracer, and although these models differ in complexity, all require knowledge of an arterial input function (AIF) to extract accurate rate constants linking the compartments.

The AIF is defined as the tracer time activity-curve (TAC) in arterial plasma and the gold standard for this measurement is invasive serial arterial blood sampling (e.g. ~1-2ml samples throughout the scan in humans). The AIF is then analysed with TACs extracted from drawing Regions of Interest (ROIs) on the desired tissues/organs to calculate tracer uptake rate constants for those tissues/organs.

In murine preclinical imaging, however, the low total blood volume (e.g. ~2ml in mice [8]) requires specialist equipment such as an arterio-venous shunt and coincidence probe [5] to extract blood samples safely, and even then may result in disturbing the system under measurement. Standard AIFs derived for a population [9] have also been suggested, although these do not account for variations in injection speed/volume or the dietary state of the animal, which may lead to poor estimation of metabolic status [10].

The AIF can be derived non-invasively by extracting an activity time course from arterial voxels on dynamic PET images [11], [12], in areas such as the carotids. Murine arteries are, however, frequently too small to be resolved on PET images [6] and therefore the small size of the mouse demands that image-derived input functions (IDIFs) be extracted from the Left Ventricular Blood Pool (LVBP) [6], [7], [13], [14]. The restricted spatial and temporal resolution of small animal PET scanners (~1-2mm FWHM) [15] makes it challenging to accurately place an ROI in the blood pool of the heart due to partial volume effects (PVE), which must be corrected for [6],

[14]. The vascular radioactivity is also blurred between tissues due to the spillover effect between hot and cold regions at low spatial resolution. This signal contamination typically reduces the IDIF peak height, increases the width of the IDIF peak and raises the tail of the curve at later time points [13]. Many methods have been developed to extract IDIFs accurately and reliably in preclinical studies, such as those based on Factor Analysis (FA) [16], which assumes that the true input function is a linear combination of the TACs extracted from both the left ventricle, right ventricle and the myocardium. These components are extracted using Principal Component Analysis (PCA). Although a robust method with good correlation to fully blood sampled curves, it requires calibration with at least one blood sample and assumes a constant, scalar relationship between the curves. Simultaneous estimation methods which take PVE and spillover into account whilst simultaneously fitting IDIFs and model parameters have also been developed [17] although the large number of parameters have led to poor reproducibility of results by other groups [18].

In humans, the geometric transfer matrix (GTM) method [19] has been successfully applied [20] to reduce PVE in the carotid arteries by segmenting them using co-registered MRI data. By using the MRI data as an anatomical prior, theoretical signal contributions for each compartment segmented using the MR data can be convolved with the point spread function (PSF) of the PET scanner and fitted to the measured signal to attain the contribution from each compartment. This was found to increase the accuracy of image derived input functions for kinetic modelling in the brain by using the blood component from the arteries as the IDIF. The drawbacks of this method have hinged on poor co-registration of PET and MR data, although the availability of combined PET/MR scanners should reduce this error by acquiring data with the subject in the same physiological state.

We believe this is the first study to reverse translate the GTM method to the mouse heart using PET and MRI data acquired sequentially. We hope to provide a gain in accuracy from the higher resolution MR data being used as an anatomical prior for the PET data, particularly as cardiac MR data is used as a gold standard measure for infarct size [1].

II. MATERIALS AND METHODS

A. *In vivo* data

Sequential PET/MRI data were analysed from twelve mice scanned as part of a study investigating a new treatment for myocardial infarction [1]. Six of these mice were treated with an experimental drug treatment (Riociguat, Bayer) and six received a placebo. No blood samples were taken from this dataset.

For all mice, MRI imaging was first performed on a 4.7T Bruker BioSpec 47/40 scanner (Bruker Inc., Ettlingen, Germany) before the animal bed was transferred to the Cambridge split-magnet PET/MR system [21], [22] for PET acquisition. The same bed configuration was used and the imaging conducted in the same session to minimize animal movement and improve the accuracy of co-registration between PET and MR datasets, as previously described [23].

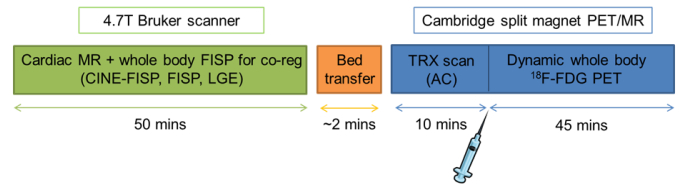


Fig. 1. Workflow of sequential PET/MR protocol

Briefly, MR imaging consisted of anatomical scans for co-registration (3D FISP, TR/TE 8/4ms, slice thickness 0.5mm, NEX = 2, 0.5mm spacing between slices, in plane resolution $120 \times 120 \mu\text{m}^2$, matrix $256 \times 256 \times 128$), cine MRI for heart function as well as late gadolinium enhancement imaging (LGE) to visualise the infarct, as detailed in [24]. The LGE MRI scan acquired 0.8mm thick slices with 0.2 mm gap and had a 256×256 matrix over a 3.5 cm field of view.

MR imaging was followed by PET imaging, with the protocol workflow summarised in Fig. 1. A 10 minute transmission scan using a ^{68}Ge source to estimate attenuation correction preceded the in-situ injection of ^{18}F -FDG. The tracer was manually administered as an intravenous bolus injection ($\sim 25\text{MBq}$) through the tail vein lasting approximately 15s, from the same cannula used for MRI contrast agent injection that ran from the mouse outside the magnet bore. It was immediately followed by a saline flush injection. PET emission data was acquired in list mode for 45 minutes.

PET images were reconstructed by 3DRP into the following dynamic frames: $12 \times 5\text{s}$, $12 \times 10\text{s}$, $12 \times 30\text{s}$, $5 \times 60\text{s}$, $5 \times 120\text{s}$ and $4 \times 300\text{s}$. A zoom factor of 2.5 was applied to give an image of matrix $128 \times 128 \times 95$ with a transaxial pixel size of 0.35mm and a slice thickness of 0.8mm. Data were normalized and calibrated with corrections for decay, detector efficiency, dead time, random events and attenuation using the vendor microPET manager software (Siemens Molecular Imaging).

Each PET image dynamic frame was subsequently binned into four cardiac motion frames to minimise heart motion and improve image quantification. The triggers used to sort the list mode data into the cardiac motion frames were derived from simultaneous ECG recordings. The end diastolic frame was identified and used for subsequent analysis, as the LVBP was largest at this stage and spillover from the myocardium was minimized. Data were also reconstructed in the same manner without cardiac gating applied to observe the blurring effect of motion on both the resulting images and IDIF results. Respiratory gating was not seen to provide improvements in the PET spatial resolution or co-registration between the PET and MR images, and so was not applied in order to preserve SNR in early dynamic frames with short durations.

B. IDIF extraction

All MRI and PET images were co-registered in MRI space using the SPMmouse toolbox [25]. Dynamic PET frames were visually inspected and no significant gross motion was observed between frames or between the MR images and different PET time frames after co-registration.

ROIs used to extract IDIFs and TACs from images were manually drawn in Analyze 8.0 using the co-registered MR images in the left ventricle region in end diastole, for both gated and ungated PET datasets. LVBP, healthy myocardium and infarcted myocardium ROIs were taken from 8 slices of

the LGE MRI images, giving full coverage of the mouse heart, with example slices showing these ROIs displayed in Fig. 2. ROIs were viewed on all PET frames and manually refined to reduce contamination from neighbouring tissue types caused by cardiac motion over the course of the dynamic scan. The mean signal from voxels within the LVBP ROI was taken as the IDIF (red in Figure 2), whilst healthy and infarcted myocardium TACs were taken as mean signal from healthy and infarcted myocardium ROIs (green and yellow respectively in Figure 2).

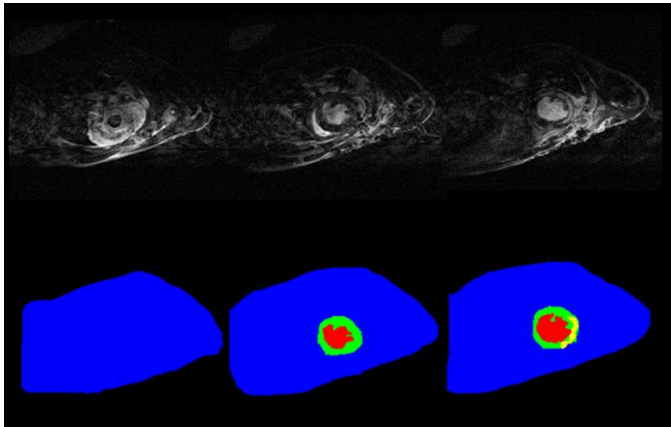


Fig. 2. Illustration of ROI regions delineated for control mouse. LVBP (red), infarct region (yellow), healthy myocardium (green), body (blue) and background (black). LVBP ROI re-sliced to match co-registered PET and used to extract IDIFs.

C. PVC IDIF extraction using the GTM method

Five ROI classes were required to conduct the GTM PVC method [19] on this mouse dataset: (a) LVBP, (b) infarcted myocardium, (c) healthy myocardium, (d) body and (e) background. The five classes were delineated from high resolution LGE MRI co-registered to the last dynamic frame of 3DRP PET images covering the mouse heart and are shown in the bottom row of Figure 2.

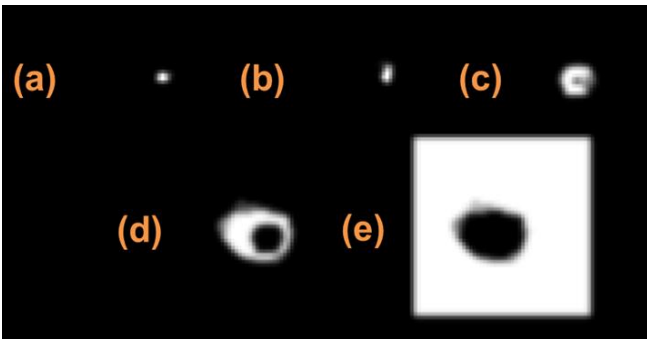


Fig. 3. PVC GTM method of IDIF determination using 5 classes: (a) LV lumen, (b) infarct, (c) healthy myocardium, (d) body and (e) background. Segmented classes are convolved with the scanner PSF. PET signal was modelled as a linear combination of these classes and the LV lumen fitted values (region (a)) were used as the corrected IDIF.

Segmented classes were convolved with a 1.8mm (FWHM) 3D isotropic Gaussian function representing the scanner PSF [21], as shown in Fig. 3. The signal from each PET frame was modelled as a linear combination of the signal from the 5

convolved ROI classes to find the corrected contributions from each region. The GTM method was applied to each dynamic PET frame individually, and so the extracted values for the LVBP coefficient (region (a) in Fig. 3) in each frame were plotted together as the corrected IDIF. The healthy and infarcted myocardium coefficients for each frame (regions (b) and (c) in Fig. 3) were used to generate their respective corrected TACs.

All whole blood IDIFs were converted to plasma IDIFs using the empirically derived relation given in equation (1) [5], [26]:

$$A_{\text{plasma}} = A_{\text{WholeBlood}} \times (0.39e^{-0.19t} + 1.117) \quad (1)$$

where A_{plasma} is the IDIF, $A_{\text{wholeblood}}$ is the activity concentration derived directly from the LVBP and t is the time during the scan.

D. Kinetic Modelling

All resulting IDIFs were then used in compartmental modelling of the mouse data using PMOD software (v2.5, PMOD technologies Inc.). A two compartment irreversible model was assumed for ^{18}F -FDG. Model biexponential curves (an accepted model for rodent AIFs [27]) were fitted to the extracted IDIFs before analysis to smooth the data.

Patlak graphical analysis [28] was performed on each IDIF and its corresponding healthy and infarcted myocardium TAC to calculate an apparent uptake constant from linear graphical analysis. K_i (the influx rate constant) was calculated using equation (2):

$$\frac{\text{TAC}(t)}{\text{AIF}(t)} = K_i \frac{\int \text{AIF}(t)}{\text{AIF}(t)} + V \quad (2)$$

The calculated K_i values for the healthy myocardium regions (calculated using uncorrected and PVC corrected IDIFs, both with and without cardiac gating applied) of both mouse groups were compared to those reported in the literature, as no blood sample data was available with this dataset to provide IDIF validation. K_i values obtained from infarcted myocardium ROIs were also compared between the treated and untreated mice groups.

III. RESULTS

A. IDIF extraction methods

Uncorrected IDIFs produced by manual ROI delineation display contamination with myocardial signal, seen from the lack of decay in the AIFs at late time points, as shown in Fig. 4 for a control mouse and Fig. 5 for a drug treated mouse.

This effect is reduced when cardiac gating is applied to the PET data, as seen in both Fig. 4 and Fig. 5, but is not eliminated. Some form of PVC is therefore essential to separate the blood and myocardium components, even when co-registered MR is available to guide the anatomical positioning of ROIs.

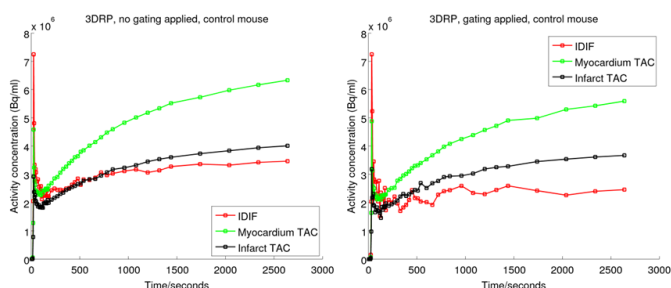


Fig. 4. IDIFs and TACs extracted for control mouse with (right) and without (left) cardiac gating applied.

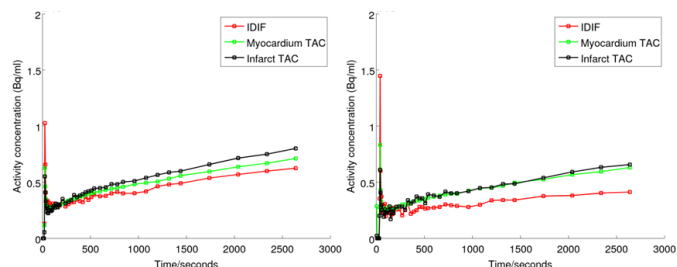


Fig. 5. IDIFs and TACs extracted for drug treated mouse with (right) and without (left) cardiac gating applied.

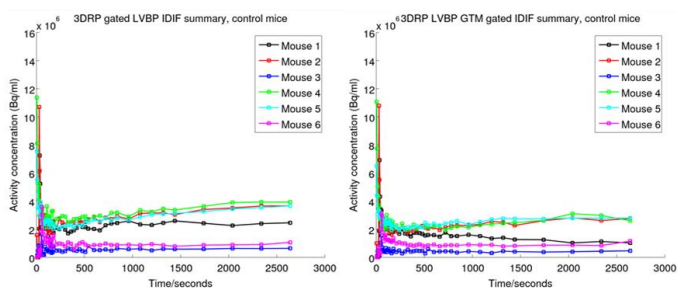


Fig. 6. IDIFs for all control mice extracted with gating applied, with (right) and without (left) GTM PVC also applied. Note that some corrected IDIFs still increase with time at later time points.

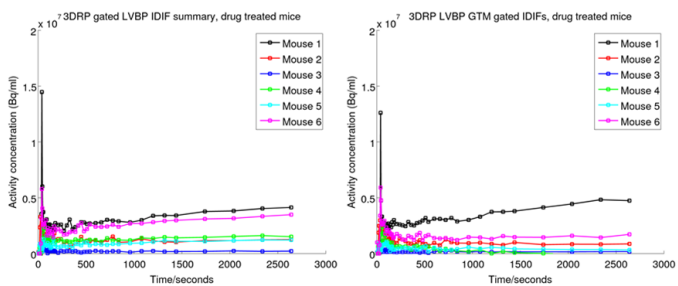


Fig. 7. IDIFs for all drug treated mice extracted with gating applied, with (right) and without (left) GTM PVC also applied. Note that some corrected IDIFs still increase with time at later time points.

IDIFs produced for the control mouse group from cardiac gated images, with and without PVC applied, are shown in Fig. 6. Corresponding IDIFs for the drug treated group are shown in Fig. 7.

The drug treated group IDIFs show greater similarity on average in their IDIF shapes compared to the control mice group, although after the application of both PVC and gating all IDIFs from both groups appear more similar as

contamination in the IDIF signals from myocardial TACs was reduced. The application of gating was shown to remove blurring due to cardiac motion in the PET data, giving more uniform IDIFs throughout both groups if gating was applied. PVC from the GTM method also reduced spillover from the myocardial TAC, giving IDIF shapes that decayed over time. This correction was increased if cardiac gating was applied in conjunction with the GTM method, as this allowed for the gated MRI data to better align with the PET data. It must be noted, however, that the GTM method is unstable and vulnerable to small errors in ROI delineation, as 2 IDIFs from the control group (Mouse 1 and Mouse 6) and 1 IDIF from the drug treated group (Mouse 1) still increase with time at later time points. This indicates that both PVE and blurring as a result of cardiac motion should be accounted for to extract accurate IDIFs and TACs for mice from the LVBVP ROI.

B. Differences between treated and untreated groups

Overlaid PET and MR images for an example mouse from each group is shown in Fig. 8. The infarcted region is identified by decreased PET tracer uptake in the untreated mouse myocardium and increased signal in LGE MRI from contrast agent uptake, indicating that a larger infarct is present, as shown previously [1]. As shown in Fig. 4 and Fig. 5, TACs for healthy and infarcted myocardium in the drug treated group are found to be similar in shape but in the control group, the infarcted tissue displayed a much lower activity concentration at late time points. This indicated a lack of viable tissue in the infarcted regions, and is consistent with the larger infarct sizes previously found in the control group using LGE MRI [1].

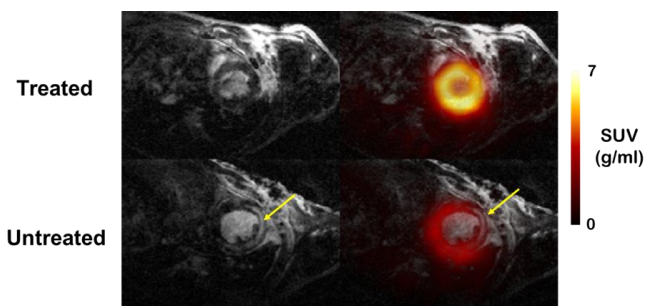


Fig. 8. Co-registered SUV PET and LGE MRI short axis views of the infarcted mouse heart. Top row: mouse treated with riociguat, bottom row: control mouse. Infarcted region (arrow) is identified by decreased PET tracer uptake in the control mouse myocardium and increased signal in LGE MRI from contrast agent uptake.

K_i values were calculated for all IDIFs and compared across the healthy and infarcted myocardium regions for both control and drug treated mouse groups, with the results for the uncorrected IDIFs shown in Table I and the GTM IDIFs shown in Table II.

The healthy myocardium region K_i values produced from all IDIFs were then compared to the literature, which reports a range between $0.08-0.22\text{ml}/\text{min}/\text{cm}^3$ [7], [26], with common values reported around $0.1\text{ml}/\text{min}/\text{cm}^3$ [6], [17], [18]. The best agreement to these values was seen with IDIFs produced using the GTM method and cardiac gating, which gave K_i values of $0.090\pm 0.041\text{ml}/\text{min}/\text{cm}^3$ for the control group and $0.096\pm 0.030\text{ml}/\text{min}/\text{cm}^3$ for the drug treated group, compared

to $0.018 \pm 0.009 \text{ ml/min/cm}^3$ for the control group and $0.014 \pm 0.021 \text{ ml/min/cm}^3$ for the drug treated group if no corrections were applied. This indicated the importance of both PVC and motion correction to IDIF extraction in this study.

TABLE I
K_i VALUES (ML/MIN/CM³), MEAN ± SD

IDIF	Healthy Myocardium		Infarcted Myocardium	
	Controls	Drug treated	Controls	Drug treated
3DRP	0.018 ± 0.009	0.014 ± 0.021	0.011 ± 0.005	0.005 ± 0.002
3DRP, gated	0.026 ± 0.014	0.025 ± 0.019	0.013 ± 0.007	0.026 ± 0.020

TABLE II
K_i VALUES (ML/MIN/CM³), MEAN ± SD

IDIF	Healthy Myocardium		Infarcted Myocardium	
	Controls	Drug treated	Controls	Drug treated
GTM	0.069 ± 0.028	0.065 ± 0.024	$0.024 \pm 0.015^*$	$0.063 \pm 0.021^*$
GTM, gated	0.090 ± 0.041	0.096 ± 0.030	$0.036 \pm 0.016^*$	$0.081 \pm 0.018^*$

*Student's t test between control and drug treated groups (n = 6), indicating significant differences in infarcted myocardium region, p value < 0.05.

These results show that the K_i values were lower in mouse hearts with larger infarcted regions visible in LGE MRI [1], with a significant difference seen between the mean K_i values for the untreated and treated groups (Student's t test, p<0.05) when using the MR ROIs with the GTM method to provide IDIFs from both gated and ungated datasets. The difference in K_i values between the groups was also more pronounced if cardiac gating and PVC from GTM were applied together, indicating that cardiac motion had a direct effect on the tracer kinetic parameters produced.

IV. DISCUSSION

IDIFs directly extracted from 3DRP reconstructed images display contamination with myocardial signal, seen from the lack of decay in the AIFs at late time points, as noted in the literature [13]. This effect was observed in this study even if cardiac gating was applied to reduce motion blurring effects and co-registered high resolution MR images were used to locate and delineate ROIs. A PVC method is therefore desirable to separate the blood and myocardium components for accurate IDIF extraction.

Importantly, only GTM PVC produced significant differences in K_i values between the treated and untreated groups, indicating that the effect of the drug may have been obscured in kinetic analysis unless PVC was applied.

The healthy myocardium K_i values calculated using both the GTM PVC method and cardiac gating the produced the best agreement with myocardial K_i values in the literature. Full

validation of this technique, however, would require comparison between the IDIFs produced to AIFs determined from serial blood sampling in future work or via a simulation study. Due to the small size of mice, gold standard AIFs from mice would most likely be determined using an MR-compatible version of an arterio-venous shunt and coincidence counter set-up [5] in a simultaneous PET/MR scanner.

The main drawback of the GTM method was its reliance on accurate ROI delineation, as even a small mismatch in ROI positioning can lead to errors in IDIFs and their corresponding K_i values, as shown in the range of PVC IDIF curve shapes produced (see Fig. 6 for the control group and Fig. 7 for the drug group) and the large variances reported in the K_i values reported. This indicated how any noise present in the IDIF results propagates into the kinetic parameters produced. The GTM method might therefore perform better if used in a simultaneous PET/MR acquisition, where co-registration errors and motion between modalities is reduced.

The GTM method also relies on the assumption that there is homogeneous uptake within each region [19] and each PET frame, which may not have been in the case for the mice where the GTM PVC method did not perform as well at reducing spillover. Another drawback of the GTM method is that it can only produce corrected IDIFs and TACs from ROIs when applied in the manner detailed in this work, and other PVC methods should be considered if corrected IDIFs and TACs are desired on a voxel by voxel basis.

V. CONCLUSIONS

We have shown that PVC is crucial for deriving IDIFs from mouse images reconstructed using 3DRP and that PVC can be provided for mice using the GTM method, which utilizes the high-resolution and excellent soft-tissue contrast of MR data to improve ROI delineation. Cardiac gating further improves these results by reducing the spillover between myocardium and LVBP. As a result of using GTM to provide PVC, significant differences in K_i values were found in the infarcted myocardium between treated and untreated mouse groups which were otherwise obscured and K_i values for the healthy myocardium agreed better with the reported values in the literature. Although this method still requires full validation against AIFs determined from serial arterial blood samples, these results suggest that kinetic modelling with combined PET and MRI may be more accurate than PET alone when blood sampling is not available, particularly in a simultaneous PET/MR scanner where co-registration errors between datasets are minimized.

REFERENCES

- [1] C. Methner, G. Buonincontri, C.-H. Hu, A. Vujic, A. Kretschmer, S. Sawiak, A. Carpenter, J.-P. Stasch, and T. Krieg, "Riociguat reduces infarct size and post-infarct heart failure in mouse hearts: insights from MRI/PET imaging.," *PLoS One*, 8 (12), p. e83910, 2013.
- [2] P. E. Kinahan and J. W. Fletcher, "Positron emission tomography-computed tomography standardized uptake values in clinical practice and assessing response to therapy.," *Semin. Ultrasound. CT. MR*, 31(6), pp. 496–505, 2010.

- [3] M. C. Adams, T. G. Turkington, J. M. Wilson, and T. Z. Wong, "A systematic review of the factors affecting accuracy of SUV measurements.," *AJR. Am. J. Roentgenol.*, 195 (2), pp. 310–320, 2010.
- [4] P. Dupont and J. Warwick, "Kinetic modelling in small animal imaging with PET.," *Methods*, 48(2), pp. 98–103, 2009.
- [5] M. F. Alf, M. T. Wyss, A. Buck, B. Weber, R. Schibli, and S. D. Krämer, "Quantification of Brain Glucose Metabolism by 18F-FDG PET with Real-Time Arterial and Image-Derived Input Function in Mice.," *J. Nucl. Med.*, 54 (1), pp. 132-138, 2013.
- [6] S. L. Thorn, R. A. Dekemp, T. Dumouchel, R. Klein, J. M. Renaud, R. G. Wells, M. H. Gollob, R. S. Beanlands, and J. N. DaSilva, "Repeatable Noninvasive Measurement of Mouse Myocardial Glucose Uptake with 18F-FDG: Evaluation of Tracer Kinetics in a Type 1 Diabetes Model.," *J. Nucl. Med.*, 54 (9), pp. 1637-1644, 2013.
- [7] M. Zhong, C. E. Alonso, H. Taegtmeier, and B. K. Kundu, "Quantitative PET Imaging Detects Early Metabolic Remodeling in a Mouse Model of Pressure-Overload Left Ventricular Hypertrophy In Vivo.," *J. Nucl. Med.*, 54 (4), pp. 609-615, 2013.
- [8] A. C. Riches, J. G. Sharp, D. B. Thomas, and S. V Smith, "Blood volume determination in the mouse.," *J. Physiol.*, vol. 228, no. 2, pp. 279–284, 1973.
- [9] P. T. Meyer, V. Circiumaru, C. A. Cardi, D. H. Thomas, H. Bal, and P. D. Acton, "Simplified quantification of small animal [18F]FDG PET studies using a standard arterial input function.," *Eur. J. Nucl. Med. Mol. Imaging*, 33, (8), pp. 948–954, 2006.
- [10] S. D. Rani, S. T. Nemanich, N. Fetti, and K. I. Shoghi, "Kinetic analysis of FDG in rat liver: Effect of dietary intervention on arterial and portal vein input.," *Nucl. Med. Biol.*, 40 (4), 537-546, 2013
- [11] P. Zanotti-Fregonara, R. Maroy, C. Comtat, S. Jan, V. Gaura, A. Bar-Hen, M.-J. Ribeiro, and R. Trébossen, "Comparison of 3 methods of automated internal carotid segmentation in human brain PET studies: application to the estimation of arterial input function.," *J. Nucl. Med.*, 50 (3), pp. 461–467, 2009.
- [12] P. Zanotti-Fregonara, K. Chen, J.-S. Liow, M. Fujita, and R. B. Innis, "Image-derived input function for brain PET studies: many challenges and few opportunities.," *J. Cereb. Blood Flow Metab.*, 31 (10), pp. 1986–1998, 2011.
- [13] R. Mabrouk, F. Dubeau, M. Bentourkia, and L. Bentabet, "Extraction of time activity curves from gated FDG-PET images for small animals' heart studies.," *Comput. Med. Imaging Graph.*, 36 (6), pp. 484–491, 2012.
- [14] L. W. Locke, M. B. Williams, K. D. Fairchild, M. Zhong, B. K. Kundu, and S. S. Berr, "FDG-PET Quantification of Lung Inflammation with Image-Derived Blood Input Function in Mice.," *Int. J. Mol. Imaging*, Article ID 356730, 6 pages, 2011, doi:10.1155/2011/356730.
- [15] A. L. Goertzen, Q. Bao, M. Bergeron, E. Blankemeyer, S. Blinder, M. Cañadas, A. F. Chatzioannou, K. Dinelle, E. Elhami, H.-S. Jans, E. Lage, R. Lecomte, V. Sossi, S. Surti, Y.-C. Tai, J. J. Vaquero, E. Vicente, D. A. Williams, and R. Laforest, "NEMA NU 4-2008 comparison of preclinical PET imaging systems.," *J. Nucl. Med.*, 53 (8), pp. 1300–1309, 2012.
- [16] R. Laforest, T. L. Sharp, J. A. Engelbach, N. M. Fetti, P. Herrero, J. Kim, J. S. Lewis, D. J. Rowland, Y. Tai and M. J. Welsch, "Measurement of input functions in rodents: challenges and solutions", *Nucl. Med. Biol.*, vol. 32, pp679-685, 2005.
- [17] Y.-H. D. Fang and R. F. Muzic, "Spillover and partial-volume correction for image-derived input functions for small-animal 18F-FDG PET studies.," *J. Nucl. Med.*, 49, (4), pp. 606–614, 2008.
- [18] L. W. Locke, S. S. Berr, and B. K. Kundu, "Image-derived input function from cardiac gated maximum a posteriori reconstructed PET images in mice.," *Mol. Imaging Biol.*, 13 (2), pp. 342–347, 2011.
- [19] O. G. Rousset, Y. Ma, and A. C. Evans, "Correction for Partial Volume Effects in PET: Principle and Validation," *J. Nucl. Med.*, 39, (5), pp 904-911, 1998.
- [20] D. Izquierdo-Garcia, J. R. Davies, M. J. Graves, J. H. F. Rudd, J. H. Gillard, P. L. Weissberg, T. D. Fryer, and E. A. Warburton, "Comparison of methods for magnetic resonance-guided [18-F]fluorodeoxyglucose positron emission tomography in human carotid arteries: reproducibility, partial volume correction, and correlation between methods.," *Stroke*, 40 (1), pp. 86–93, 2009.
- [21] R. C. Hawkes, T. D. Fryer, A. J. Lucas, S. B. Siegel, R. E. Ansonge, J. C. Clark, and T. A. Carpenter, "Initial Performance Assessment of a Combined microPET @ Focus-FI20 and MR Split Magnet System," *IEEE Nucl. Sci. Symp. Conf. Rec.*, pp. 3673–3678, 2008
- [22] A. J. Lucas, R. C. Hawkes, P. Guerra, R. E. Ansonge, R. E. Nutt, J. C. Clark, T. D. Fryer, and T. A. Carpenter, "Development of a combined microPET @ -MR system," *IEEE Nucl. Sci. Symp. Conf. Rec.*, pp. 2345–2348, 2006.
- [23] G. Buonincontri, C. Methner, T. A. Carpenter, R. C. Hawkes, S. J. Sawiak and T. Krieg, "MRI and PET in mouse models of myocardial infarction", *J. Vis. Exp.*, vol. 82, e50806, 2013, doi:10.3791/50806
- [24] G. Buonincontri, C. Methner, T. Krieg, T. A. Carpenter and S. J. Sawiak, "A fast protocol for infarct quantification in mice", *J. Magn. Resonance Imaging*, vol. 38, no. 2, pp468-473, 2013
- [25] S. J. Sawiak, N. I. Wood, G. B. Williams, A. J. Morton and T. A. Carpenter, "SPMmouse : A new toolbox for SPM in the animal brain," in *Proc. Intl. Soc. Mag. Reson. Med.*, p. 1086, 2009.
- [26] G. Z. Ferl, X. Zhang, H.-M. Wu, M. C. Kreissl, and S.-C. Huang, "Estimation of the 18F-FDG input function in mice by use of dynamic small-animal PET and minimal blood sample data.," *J. Nucl. Med.*, 48 (12), pp. 2037–2045, 2007.
- [27] E. Poulin, R. Lebel, E. Croteau, M. Blanchette, L. Tremblay, R. Lecomte, M. Bentourkia, and M. Lepage, "Conversion of arterial input functions for dual pharmacokinetic modeling using Gd-DTPA/MRI and 18F-FDG/PET.," *Magn. Reson. Med.*, 69 (3), pp. 781–792, 2013.
- [28] C. S. Patlak, R. G. Blasberg, and J. D. Fenstermacher, "Graphical evaluation of blood-to-brain transfer constants from multiple-time uptake data.," *J. Cereb. Blood Flow Metab.*, 3 (1), pp. 1–7, 1983.